Journal of Sound and Vibration (1997) **205**(2), 167–184

MEASUREMENTS OF ISOTHERMAL COMPLEX MODULI OF VISCOELASTIC MATERIALS OVER A LARGE RANGE OF FREQUENCIES

M. Soula, T. Vinh, Y. Chevalier, T. Beda and C. Esteoule

Rheology and Structure Group, *Institut Supérieur des Matériaux et de la Construction Mécanique* (*ISMCM*), 93407-*Saint-Ouen cedex*, *France*

(*Received* 15 *July* 1996, *and in final form* 21 *February* 1997)

A method of determination of the Young's and shear complex moduli of viscoelastic materials using a transmissibility function is presented. The experimental set-up shows that it is possible to evaluate both moduli on the same samples. We will show that, with appropriate inverse methods, isothermal complex moduli are obtained over a large range of frequencies.

1. INTRODUCTION

The determination of the Young's and shear complex moduli of beams has given rise to an abundant literature since 1950. Most of the commercially available apparatus uses off-resonance methods in which the vibrating sample is assimilated to a one-degree-of-freedom mechanical system. The evaluation of complex stiffness allows the determination of complex moduli. This method imposes drastic validity conditions: for example, short sample in tension–compression tests to avoid buckling, and a restricted range of frequency which covers less than one decade of frequency. To obtain a larger range of frequency, the Williams–Landel–Ferry method using the equivalence principle between temperature and frequency [1] is referred to. Often force and displacement (or acceleration) are measured and this raises the problem of the stiffness of the load frame [2], which is finite and has an influence on the measurements themselves. Correction factors due to test fixture, stiffness and inertia have been proposed [2, 3].

The difficulty of taking into account the real boundary conditions imposed on a short sample, with respect to the ideal boundary conditions, constitutes an obstacle in many cases for obtaining the correct value of the complex modulus; to mention one example, the three-point bending test in which short samples are often used and shear deformation is neglected. Moreover, damping measurements in this method are affected by large errors due to the contacts and Coulomb friction between the knife edges and sample.

Pritz [4] used the Love theory of longitudinal vibration of a viscoelastic rod to evaluate the complex Young's modulus. The geometric dispersion of the phase velocity (i.e., its dependence on the frequency) due to the finite dimensions of the rod and the viscoelastic dispersion, due to the material itself, are taken into account. The practical application of this study resides in the range of frequency in which the so-called apparent Young's modulus is valid, if the lateral dimension of the sample is accounted for. Read and Dean

0022–460X/97/320167 + 18 $25.00/0/sv970978

[5], adopting considerations similar to those of Pritz, proposed correcting factors for complex moduli in different kinds of vibrations (longitudinal, flexural, etc.).

Oyadiji and Tomlinson [6] have presented resonance and non-resonance methods using longitudinal vibrations. With the resonance method, from the complex transmissibility function, defined as the quotient of output to input displacements (or velocities or accelerations), the complex Young's modulus at the first four resonance frequencies was evaluated with a low mass at the output. The non-resonance method valid for low frequencies requires a correction shape factor for evaluation of the Young's modulus. The frequency range does not exceed 100 Hz.

Lundberg and Blanc [7] used progressive longitudinal waves created by impacts on long rods. Two methods utilized strains and particle velocities respectively. Discussions concerned various cases of reflection coefficient of waves. The range of frequencies for the evaluation of the Young's modulus was between 0·2 and 10 kHz. The materials tested were Nylon and vulcanized rubber.

Ödeen and Lundberg [8] proposed a method in which impact on a rod specimen permitted the evaluation of the complex modulus from measured end-point accelerations. Stationary waves were created in the samples. The materials used were polyamide and polypropylene. The range of frequencies extended from 300 Hz to 10 000 Hz.

Beda [9] used an experimental set-up similar to that of Ödeen and Lundberg, but the excitation signal was white noise instead of impacts. The Newton–Raphson method permits the evaluation of complex roots of transcendental functions of the complex variables from which the complex Young's modulus is deduced. The range of frequencies is similar to that obtained by Ödeen and Lundberg [8].

Jimenez and Uberal [10] decomposed the response of the viscoelastic rod into a sum of individual resonances. The transfer function is represented as a meromorphic function of frequency with complex poles. However, the authors adopted the hypothesis of very low damping of the material to evaluate real poles. In the concept of an inverse problem, the proposed method is similar to that used in classical modal analysis.

The first part of this paper is devoted to the identification problem. We will present two classes of methods of finding complex roots of transcendental functions deduced from the transmissibility function. All of the methods presented below are used by us to evaluate the Young's and shear complex moduli.

In the second part, the experimental set-up and some experimental results will be presented and discussed.

2. IDENTIFICATION OF COMPLEX MODULI FROM DYNAMIC RESPONSE OF THE VISCOELASTIC SAMPLE

The sample, of length L, with two accelerometers attached to its ends, is shown schematically in Figure 1. Let M_1 and M_2 be their masses. At $x = 0$, the rod is excited by a white noise acceleration. If the wavelength λ of the stationary waves created in the rod specimen is much larger than the lowest transverse dimension D of the rod.

$$\lambda/D \gg 10, \tag{1}$$

the one-dimensional elementary theory of longitudinal vibration of rod can be used [4, 9, 11]. With the boundary conditions at both ends taken into account, the Fourier transform of the equation of motion is

$$E^*(\omega)\, \partial^2 u^*(x, \omega)/\partial x^2 = -\rho\omega^2 u^*(x, \omega), \tag{2}$$

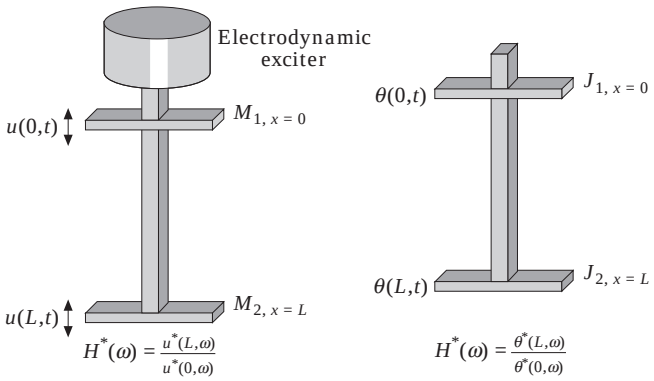

Figure 1. (a) The longitudinal vibration of a rod with two attached accelerometers to its ends. (b) The torsional vibration of a rod with two inertias attached to its ends.

where $u^*(x, \omega)$ is the Fourier transform of the displacement u at abscissa x, ω is the angular frequency and $E^*(\omega)$ is the complex Young's modulus (a list of nomenclature is given in Appendix C). The Fourier transform of u is defined as

$$u^*(x, \omega) = \int_{-\infty}^{+\infty} u(x, t)\, \mathrm{e}^{-\mathrm{j}\omega t}\, \mathrm{d}t. \tag{3}$$

The constitutive equation relating axial stress σ_{xx} and the axial strain ε_{xx} for viscoelastic material is a Stieljes convolution,

$$\sigma_{xx}(x, t) = \frac{\mathrm{d}}{\mathrm{d}t} \int_0^t E_r(\tau)\varepsilon_{xx}(x, t - \tau)\, \mathrm{d}\tau, \tag{4}$$

where $E_r(\tau)$ is the time relaxation function. If one takes the Fourier transforms of both members in equation (4), one has

$$\sigma_{xx}^*(x, \omega) = \mathrm{j}\omega E_r^*(\omega)\varepsilon_{xx}^*(x, \omega), \qquad \sigma_{xx}^*(x, \omega) = E^*(\omega)\varepsilon_{xx}^*(x, \omega). \tag{5, 6}$$

The Young's complex modulus $E^*(\omega)$ used in equations (6) and (2), is in view of equation (4) the Fourier transform of the time derivative of the relaxation function:

$$\mathbf{F}^{-1}[E^*(\omega)] = \mathrm{d}E_r(t)/\mathrm{d}t. \tag{7}$$

The transmissibility function is defined as the quotient of the Fourier transforms of output acceleration $\ddot{u}(L, t)$ and input acceleration $\ddot{u}(0, t)$:

$$H^*(\omega) = \mathbf{F}[\ddot{u}(L, t)]/\mathbf{F}[(\ddot{u}(0, t)]. \tag{8}$$

$H^*(\omega)$ is evaluated as

$$H^*(\omega) = 1/\{\cos(\beta^*) - \gamma_2\beta^* \sin(\beta^*)\}, \tag{9}$$

in which γ_2 is defined as the quotient of the mass of the second accelerometer to the mass of the rod:

$$\gamma_2 = M_2/\rho SL \tag{10}$$

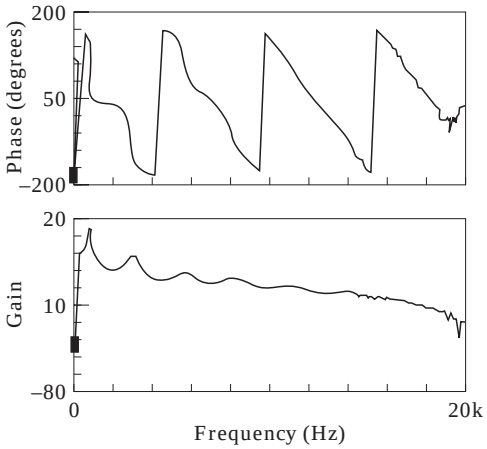

Figure 2. The experimental transmissibility function $H^*(f)$ of polyamide 6 (PA6), phase and gain (circular cross-section, diameter 10·5 mm and length $L = 200$ mm; longitudinal vibration tests).

and

$$u^*(x, t) = (A \cos(\beta^* x/L) + B \sin(\beta^* x/L))\, e^{j\omega t}. \tag{11}$$

Bringing equation (11) into equation (2) yields

$$\beta^{*2} = \rho\omega^2 L^2/E^*(\omega), \tag{12}$$

or

$$\beta^* = (\omega L/|v|) \exp(-j\delta/2), \tag{13}$$

$$|v| = [|E^*|/\rho]^{0\cdot5}, \qquad |E^*| = [(\mathscr{R}e\, E^*)^2 + (\mathscr{I}m\, E^*)^2]^{0\cdot5},$$

$$\text{tg}\, \delta = \mathscr{I}m\, E^*/\mathscr{R}e\, E^*. \tag{14}$$

It is more convenient, due to equation (9), to use the reciprocal of $H^*(\omega)$:

$$1/H_E^*(\omega) = T^*(\omega) = \cos\beta^* - \gamma_2\beta^* \sin\beta^*. \tag{15}$$

The identification problem consists of evaluating $E^*(\omega)$ for a given angular frequency ω, the complex quantity of the first member of equation (13) being known.

An example of the experimental transmissibility function $H^*(\omega)$ obtained from tests on polyamide 6 (PA6) is given in Figure 2.

2.1. NEWTON–RAPHSON METHODS

2.1.1. *First method*

Equation (15) can be decomposed into two functions, $f_1(\beta_1, \beta_2)$ and $f_2(\beta_1, \beta_2)$, of two real variables β_1, and β_2. One has, from equation (12),

$$\beta^* = \beta_1 - j\beta_2, \tag{16}$$

$$f_1(\beta_1, \beta_2) = \mathscr{R}e\,(T^*) - \cos(\beta_1)\cosh(\beta_2) + \gamma_2\beta_1 \sin(\beta_1)\cosh(\beta_2) - \gamma_2\beta_2 \cos(\beta_1)\sinh(\beta_2), \tag{17}$$

$$f_2(\beta_1, \beta_2) = \mathscr{I}m\,(T^*) - \sin(\beta_1)\sinh(\beta_2) - \gamma_2\beta_1 \cos(\beta_1)\sinh(\beta_2) - \gamma_2\beta_2 \sin(\beta_1)\cosh(\beta_2). \tag{18}$$

The first method allows the calculation of increments of β_1 and β_2:

$$\Delta\beta_1 = \beta_1^{i+1} - \beta_1^i = \frac{-f_1 f_{2,\beta_2} - f_2 f_{1,\beta_1}}{f_{1,\beta_1} f_{2,\beta_2} - f_{2,\beta_1} f_{1,\beta_2}}, \tag{19}$$

$$\Delta\beta_2 = \beta_2^{i+1} - \beta_2^i = \frac{f_1 f_{2,\beta_1} + f_2 f_{1,\beta_1}}{f_{1,\beta_1} f_{2,\beta_2} - f_{2,\beta_1} f_{1,\beta_2}}. \tag{20}$$

The subscript β's in equations (19) and (20) after the comma denote the derivatives with respect to the variable concerned.

2.1.2. *Second method*

The second method makes direct use of equation (15), which is written in the form

$$f(\beta^*) = T^* - \cos\beta^* + \gamma_2\beta^* \sin\beta^* = 0. \tag{21}$$

$f(\beta^*)$ is considered as a function of the complex variable β^* and the Newton–Raphson formula gives

$$\beta^{*i+1} = \beta^{*i} - \frac{f(\beta^{*i})}{f_{,\beta^{*i}}(\beta^{*i})}, \qquad f_{,\beta^{*i}} = \frac{\partial f}{\partial \beta^{*i}} = \frac{\partial(\mathrm{Re}\, f)}{\partial \beta_1^i} + \mathrm{j}\,\frac{\partial(\mathrm{Im}\, f)}{\partial \beta_1^i}. \tag{22, 23}$$

The superscript i designates the value of β^* at the angular frequency ω_i; see equation (13).

The experimental transmissibility curve $H^*(\omega)$ is obtained as a function of ω and β^*. Equation (13) shows that β^* is function of three variables: ω, $|v|$ and the damping angle δ. One can write the first derivative of f in equation (21) as

$$\frac{\mathrm{d}f}{\mathrm{d}\beta^*} = \frac{\partial f}{\partial\omega}\frac{\partial\omega}{\partial\beta^*} + \frac{\partial f}{\partial v}\frac{\partial v}{\partial\omega}\frac{\partial\omega}{\partial\beta^*} + \frac{\partial f}{\partial\delta}\frac{\partial\delta}{\partial\omega}\frac{\partial\omega}{\partial\beta^*}. \tag{24}$$

In the two last terms of equation (24), the variations of the velocity v and the damping angle δ versus the angular frequency ω are very low, so one can neglect them and retain for the first derivative the first term in equation (24):

$$\mathrm{d}f/\mathrm{d}\beta^* \cong (\partial f/\partial\omega)(\partial\omega/\partial\beta^*). \tag{25}$$

The main difficulty when using equation (22) to find the root β^* in equation (21) resides in the fact that $H^*(\omega)$ includes many maxima (resonance) and minima (antiresonance); see Figure 2. The number of extrema is related to the damping of the sample. In equation (22) the second term tends to infinity when $f(\beta^*)$ reaches an extremum.

2.1.3. *Improvements for the second method*

If no caution is taken, Newton–Raphson formula (22) inevitably gives rise to oscillations for β_1 as well as β_2, and consequently unadmissible oscillations of the curve of the complex modulus E^* (see equation (12)) are obtained. An example of such kinds of calculations of the complex Young's modulus of polyamide 6 (PA6) is shown in Figure 3. Ödeen and Lundberg [8] obtained similar results with oscillations. Curve-fitting is not a good solution to obtain monotonic curves. An improved complex Newton–Raphson method is as follows.

In equation (22), one has to discard frequencies corresponding to resonances and antiresonances. At a resonance frequency the real part of T^* goes to zero, and equation (17) is rewritten as

$$-\cos(\beta_1)\cosh(\beta_2) + \gamma_2\beta_1 \sin(\beta_1)\cosh(\beta_2) - \gamma_2\beta_2\cos(\beta_1)\sinh(\beta_2) = 0. \tag{26}$$

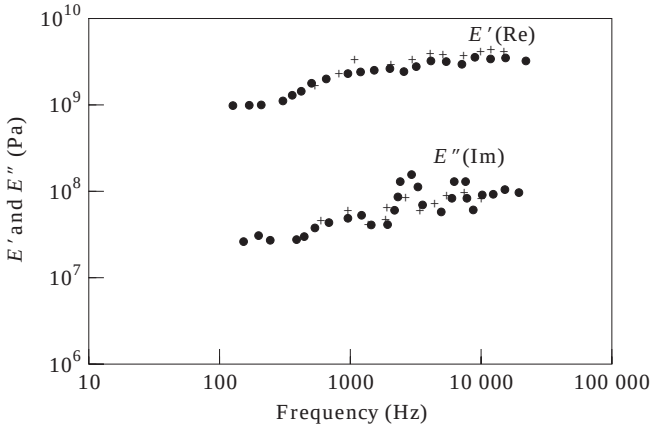

Figure 3. The complex Young's modulus obtained by complex Newton–Raphson, second method equation (22); material, polyamide 6 (PA6). . . . . , Parasitic oscillations are present on both curves; + + + + +, Ödeen and Lundberg [8] obtained similar results on the same material.

The imaginary part reaches a maximum:

$$\mathcal{I}m\,(T^*) - \sin(\beta_1)\sinh(\beta_2) - \gamma_2\beta_1\cos(\beta_1)\sinh(\beta_2) - \gamma_2\beta_2\sin(\beta_1)\cosh(\beta_2) = 0. \quad (27)$$

Equations (19) and (20) are reduced to

$$\Delta\beta_1 = \beta_1^{i+1} - \beta_1^i = \frac{f_1 f_{2,\beta_2}}{f_{2,\beta_1} f_{1,\beta_2}}, \qquad \Delta\beta_2 = \beta_2^{i+1} - \beta_2^i = \frac{f_1 f_{2,\beta_1}}{-f_{2,\beta_1} f_{1,\beta_2}}. \quad (28, 29)$$

Equations (28) and (29) allow the evaluation of β_r^* at a resonance frequency.

At antiresonance frequencies, equations (17) and (18) are rewritten with the imaginary part of T^* equal to zero. Equations (19) and (20) are reduced to

$$\Delta\beta_1 = \beta_1^{i+1} - \beta_1^i = \frac{-f_2 f_{1,\beta_1}}{f_{1,\beta_1} f_{2,\beta_2}}, \qquad \Delta\beta_2 = \beta_2^{i+1} - \beta_2^i = \frac{f_2 f_{1,\beta_1}}{f_{1,\beta_1} f_{2,\beta_2}}. \quad (30, 31)$$

Equations (30) and (31) allow one to evaluate the root β_{ar}^* at an antiresonance frequency.

Calculations of complex moduli through resonance and antiresonance frequencies are possible by using equation (22) if the frequency range is decomposed into intervals excluding resonance and antiresonance frequencies. In each of these intervals, $T^*(\omega)$ varies monotonically and calculations based on equation (22) give rise to a complex modulus curve with reduced oscillations. In the last section of the paper, the application of the two Newton–Raphson methods will be presented.

3. NEW METHOD OF COMPLEX MODULUS COMPUTATION BY USING AN ADAPTED BLACK'S CHART

Black's chart, a popular method in control engineering, is the curve of amplitude of the transmissibility (evaluated in decibels) versus the phase angle Φ between input and output signals. This graphical representation of $|T^*|$ (in dB) *vs*. Φ (in degrees) is adapted here to equation (21).

The two families of curves are contours of equal β_1 (the real part of β^*) and contours of equal β_2 (the imaginary part of β^*) respectively; see equation (16).

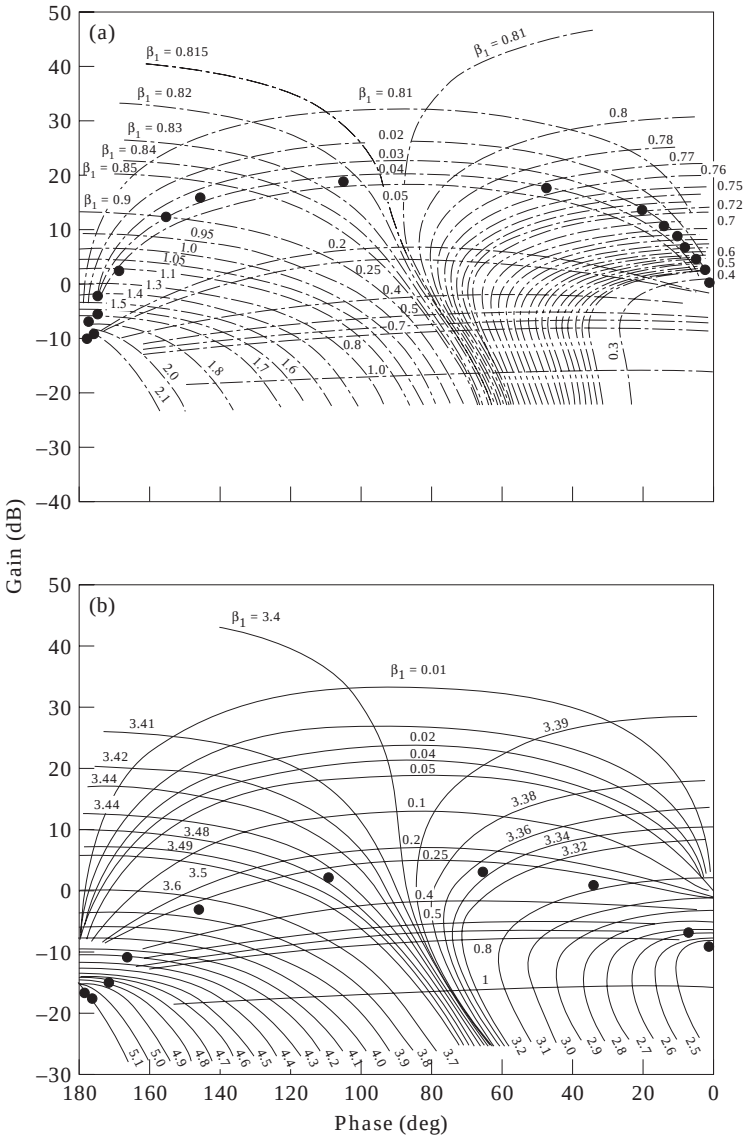

Figure 4. Black's chart adapted to the longitudinal vibration of a rod, Abscissa phase angle Φ, ordinate gain (in dB). Two families of curves are represented: $\mathscr{R}e\,[\beta^*] = \beta_1$ and $\mathscr{I}m\,[\beta^*] = \beta_2$ and allow direct evaluation of complex modulus. (a) First mode; (b) second mode; ●, experimental results.

Such charts, corresponding respectively to the two first resonance zones, are presented in Figures 4(a) and (b). For a set of values (β_1, β_2) it is easy to evaluate from equations (17) and (18) the amplitude T^* and the phase Φ.

The presence of hyperbolic functions in equations (17) and (18) makes the chart non-symmetric with respect to the phase angle Φ. Consequently, the preliminary calculations permitting the graphical representation must be carried out for each vibration mode independently.

The experimental curve T^* in gain and phase is graphically superposed on the Black's chart. By interpolation one obtains easily the set of value, β_1 and β_2 for given values of angular frequency ω, $|T|$ and phase Φ.

4. CORRECTION OF COMPLEX YOUNG'S MODULUS TAKING INTO ACCOUNT THE ROD LENGTH, THE TRANSVERSE INERTIA AND THE TRANSVERSE SHEAR

One of the weaknesses of the elementary theory of longitudinal rod vibration is that, for the elastic case, there is no geometric dispersion of the phase velocity, defined as

$$v = (E/\rho)^{0.5}. \tag{32}$$

This approximation is valid for very long wavelengths. With increasing frequency, equation (32) is not valid and one has to replace elementary theory by more refined theory [12]. The majority of researchers used Love theory [3, 4] which takes into account only the inertia effect and not the shear effect. To obtain a more general correction formulae, Bishop's equation [12] takes both effects into account, and consequently is more appropriate over a large range of frequencies. Read and Dean [5] presented appropriate formulae for correction; the equations to be presented here constitute improvements on those they proposed.

Bishop's equation of longitudinal elastic rod vibratoin is, r being the radius of gyration, G the shear modulus and v the Poisson ratio,

$$\rho\,\partial^2 u/\partial t^2 - E\,\partial^2 u/\partial x^2 - \rho v^2 r^2\,\partial^4 u/\partial x^2\,\partial t^2 + G v^2 r^2\,\partial^4 u/\partial x^4 = 0. \tag{33}$$

For a viscoelastic rod in the harmonic regime, one has

$$-\rho\omega^2 u^* - E^*\,\partial^2 u^*/\partial x^2 + \rho v^2 \omega^2 r^2\,\partial^2 u^*/\partial x^2 + G^* v^{*2} r^2\,\partial^4 u^*/\partial x^4 = 0. \tag{34}$$

Equation (33) is the fourth order with respect to the x. The solution of equation (34) is a linear combination of trigonometric functions and hyperbolic functions. Closed form solutions for elastic rods exist [12]. Their computation is tedious. The additional difficulty resides in the simultaneous presence of the Young's and shear complex moduli as well as the Poisson ratio. If one admits that E^* and G^* are two complex variables, the problem is practically intractable. For viscoelastic isotropic material, one can reasonably hypothesize that the Poisson ratio is nearly constant, real and practically independent of frequency. Equation (34) can be simplified by adopting

$$G^* = E^*/2(1 + v). \tag{35}$$

In Appendix B additional comments concerning the Poisson ratio are provided.

In equation (34) one has only one complex variable E^*, v being known. Instead of using a closed form solution for equation (34), the following approximation is suggested.

The phase velocity v_B corresponding to Bishop's equation and the phase velocity for elementary theory v_E are evaluated by using progressive wave for a semi-infinite rod,

$$u^*(x, \omega) = U_0 \exp(\mathrm{j}\omega t - \mathrm{j}k^* x), \tag{36}$$

with complex phase velocity defined as

$$v^* = \omega/k^*. \tag{37}$$

Bringing equation (36) into equation (33) yields

$$E_b^* = E_a^* \frac{1 + v^2 r^2 k_a^{*2}}{1 + v^2 r^2 k_a^{*2}/2(1 + v)},$$

with $k^* = \beta^*/L$. Subscript a refers to an apparent experimental value obtained with elementary theory:

$$E_b^* = E_a^* \frac{1 + v^2 r^2 \beta^{*2}}{1 + v^2 r^2 \beta^{*2}/2(1+v)L^2}. \tag{38}$$

E_b^* is the corrected complex modulus with three corrections (inertia, shear and length).

5. SHEAR COMPLEX MODULUS

By using the same sample and choosing an appropriate excitation, it is possible to evaluate the complex shear modulus. In Figure 1(b) is shown a schematic diagram of the sample excited in torsion at the upper end of the sample. A specimen which is maintained vertical is not subject to parasitic flexural vibrations by using an appropriate mechanical device. Two contactless angular displacement transducers are used here to avoid additional damping due to cable connections.

5.1. EQUATION OF MOTION

The Saint-Venant elementary torsional vibration theory is used:

$$C_T \, \partial^2\theta/\partial x^2 = \rho I_p \, \partial^2\theta/\partial^2 t. \tag{39}$$

C_T is the torsion stiffness given by, G being the shear modulus,

$$C_T = KG. \tag{40}$$

For a circular cross-section,

$$K = I_p = \pi R^4/2,$$

where I_p is the polar second moment of area of the rod. For a rectangular cross-section, warping is taken into account. Saint-Venant's theory gives

$$K = bh^3\xi(c), \tag{41}$$

where b is the width, h is the thickness and $c = b/h$. $\xi(c)$ is given by the series

$$\xi(c) = \tfrac{1}{3} - \frac{64}{\pi^5 c} \sum_{n=0}^{\infty} \frac{1}{(2n+1)^5} \operatorname{th}\left(\frac{(2n+1)\pi c}{2}\right), \tag{42}$$

where th designates the hyperbolic tangent. The series (42) has fast convergence.

In the harmonic regime equation (39) is as

$$C_T^* \, \mathrm{d}^2\theta^*(x)/\mathrm{d}x^2 = -\rho\omega^2 I_p \theta^*(x), \qquad C_T^* = KG^*. \tag{43, 44}$$

Comparing equation (43) to equation (2), one can say that the equations of motion are similar. The boundary conditions are also similar, if one replaces the additional mass M_2 at the free end by an additional rotational inertia I_2 for torsional forced vibration.

Consequently, one can use the methods previously presented and discussed to evaluate the shear complex modulus.

5.2. CORRECTION OF SHEAR COMPLEX MODULUS

One has to replace the elementary Saint-Venant's theory of rod torsion by Barr's theory [13], which is valid only in the case of a non-circular cross-section. For a circular cross-section, there is no velocity geometric dispersion at all and consequently, in this case, no correction is necessary.

Barr's equation of motion in the elastic case is

$$\chi^2 \frac{\partial^4 \theta}{\partial x^4} - \left(\frac{\rho}{G} + \frac{\rho \chi^2}{E}\right) I_p \frac{\partial^4 \theta}{\partial x^2 \, \partial t^2} - \frac{K(1-K)G}{\mu^2} \frac{\partial^2 \theta}{\partial x^2} + \frac{\rho(1-K)}{\mu^2 E} \frac{\partial^2 \theta}{\partial t^2} + \frac{\rho^2}{EG} \frac{\partial^4 \theta}{\partial t^4} = 0, \quad (45)$$

where E and G are the Young's and shear moduli and χ is a coefficient introduced to adjust the asymptotic behaviour of the wave velocity when the frequency goes to infinity. χ depends on the Poisson ratio. μ is a factor introduced to take into account the transverse dimension of the sample. Its expression is given in Appendix A.

K, present in equations (40) and (41), takes into account the warping of the cross-section. As for longitudinal waves, one can use the approximation using progressive torsional wave for the correction of the shear complex modulus. In the harmonic regime equation (45) is rewritten as

$$\theta^*(x, \omega) = \theta_0 \exp(\mathrm{j}\omega t - k^* x). \quad (46)$$

Bringing expression (46) into equation (45) yields the following correction for the complex shear modulus (G_a^* is the apparent modulus deduced from equation (39) and G_c^* is the corrected modulus):

$$G_c^* = G_a^* \frac{1 + \dfrac{2 + (1+\nu) + \chi^2}{1-K} \mu^2 k^* - \dfrac{KL^2}{(1-K)} k^{*2}}{1 + \dfrac{2 + (1+\nu)\chi^2}{K(1-K)} \mu^2 k^{*2}}. \quad (47)$$

For viscoelastic material, k and G^* become complex quantities in equation (45):

$$k^* = \beta^*/L, \qquad G^* = \rho\omega^2 L^2/\beta^{*2},$$

where L is the length of the sample.

Note that in equation (47) if one sets the term $\{KL^2/(1-K)\}k^{*2}$ equal to zero, one obtains the correction formula proposed by Read and Dean [5].

6. THE EXPERIMENTAL SET-UP

In a climatic box, see Figure 5, the temperature of which can be adjusted from -100°C to $+100^\circ$C, two vertically suspended samples were used respectively to measure the complex Young's modulus by using stationary longitudinal waves (on the right) and the complex shear modulus by using stationary torsional waves (on the left).

Long rods were used so as to adopt a one-dimensional elementary theory of vibrations. The upper end of the right specimen was connected to an electrodynamic exciter. The excitation signal is a broadband white noise. The lower end was free and connected to a mass M_2, which was the mass of the second accelerometer.

A second electrodynamic exciter, the moving coil of which acts horizontally, applied through a lever a torsional displacement to the sample. Two displacement transducers were connected to two additional torsional inertia and measured the excitation and the response of the rod. Contactless transducers were used here so as to avoid connections with cables which would strongly influence damping measurement and also would introduce additional stiffness with respect to the low stiffness of the specimen, if measurements were made on soft elastomers.

The reciprocal of the transmissibility function T^* (equation (15)) was directly evaluated by a two-channel analyzer. A microcomputer with special programs for finding roots β^*

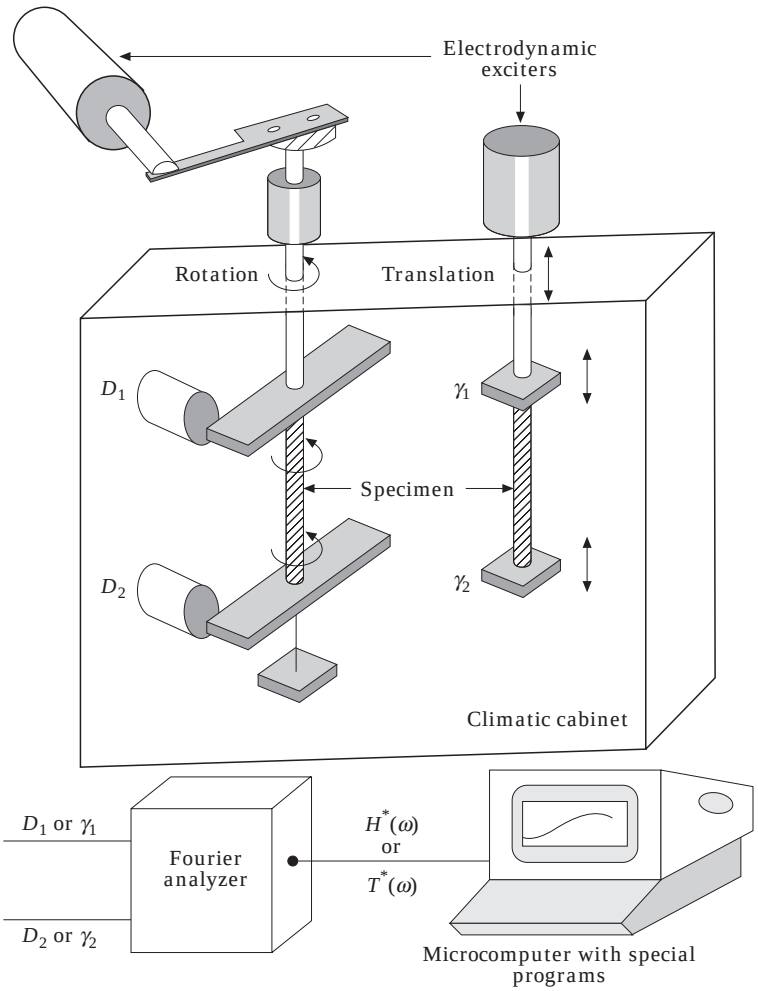

Figure 5. In a climatic chamber: on the right, longitudinal vibrations at both ends of the specimen are measured by two accelerometers γ_1 and γ_2; on the left, torsional vibration of the specimen, angular oscillations D_1 and D_2 at both ends, are measured by contactless displacement transducers. The electronic set-up is not presented. The Fourier analyzer furnishes $H^*(\omega)$ or $T^*(\omega)$. Special programs on a microcomputer give $E^*(\omega)$ or $G^*(\omega)$.

permitted one to obtain the complex Young's modulus E^* and/or the complex shear modulus G^*.

By varying the temperature of the specimen, one could extend the frequency range to more than six decades using the Williams–Landel–Ferry method [1].

7. RESULTS

Three examples of complex moduli measurements are presented.

7.1. TESTS ON A SOLID PROPELLANT

The material is a viscoelastic and high damping material. The first Newton–Raphson method presented in section 2.1 is used here with two real variables β_1 and β_2.

The real and imaginary curves for $T^*(\omega)$ are presented in Figure 6. The frequency range goes from 30 Hz to 7000 Hz. With a piezoelectric exciter one can extend the higher frequency beyond 10 000 Hz; see Figure 6(b).

For this material the first Newton–Raphson method with two real variables β_1 and β_2 was used. This method is stable and gives rise to a monotonically increasing Young's modulus E^*. In Figure 7, the real and imaginary parts of E^* are presented.

7.2. TESTS ON ELASTOMERS WITH VARIOUS DAMPING COEFFICIENTS

7.2.1. *High damping elastomers*

Figures 8(a and b) show the transmissibility $H^*(f)$ in gain and phase versus the frequency f. Note that one has to unfold the phase curve. Each portion of this curve must be situated in the right quadrant and not necessarily between $(-\pi, +\pi)$ as usual. The second Newton–Raphson method was used here with β^* as a complex variable.

The absolute value of Young's modulus E^* and the damping coefficient $\tan \delta_E$ in the range of frequency 30–7000 Hz are shown in Figures 9(a) and (b).

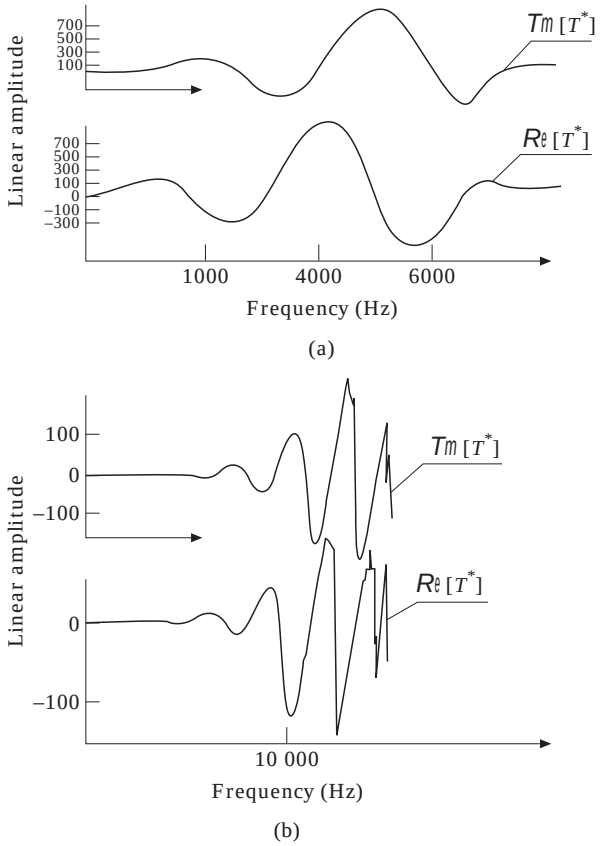

Figure 6. Tests on solid propellant using longitudinal vibrations. (a) With electrodynamic exciter; (b) with piezoelectric exciter. Linear representations of real and imaginary parts of $T^*(f)$; calculation of $T^*(f)$ by first Newton–Raphson method, equations (28) and (29).

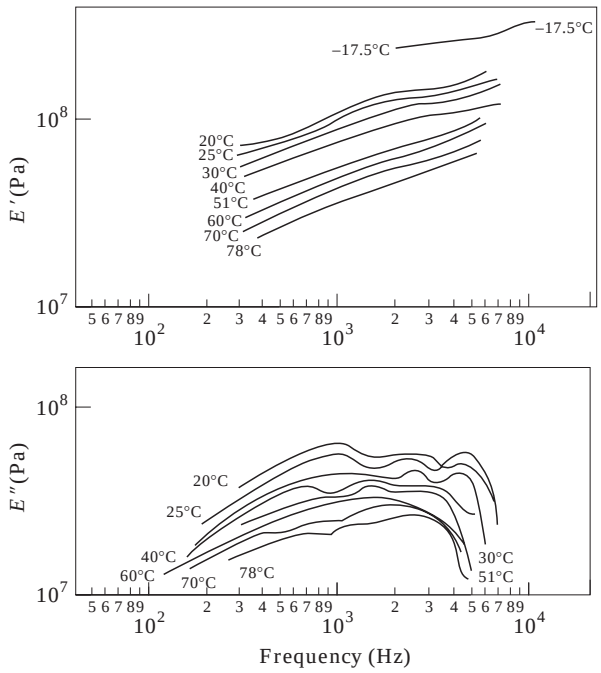

Figure 7. Test on solid propellant at various temperatures. (a) Real Part $E'(f)$ of Young's modulus; (b) imaginary part $E''(f)$.

7.2.2. *Low damping elastomers*

In Figures 8(c) and (d) are shown the curves of the transmissibility function. Attention is focused on the presence of five resonance frequencies. The Young's modulus is presented in Figure 10. The existence of many successive transition zones is visible on the t$g\ \delta_E$ curve

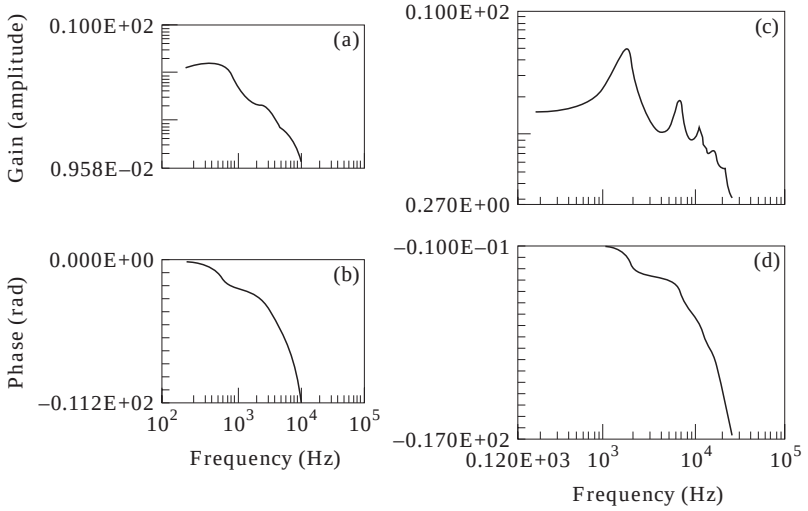

Figure 8. High damping elastomer: transfer function (a) amplitude and (b) phase versus frequency; the phase representation has to be unfolded from curve drawn between $\pm\pi$. Low damping elastomer: (c) gain; (d) unfolded phase.

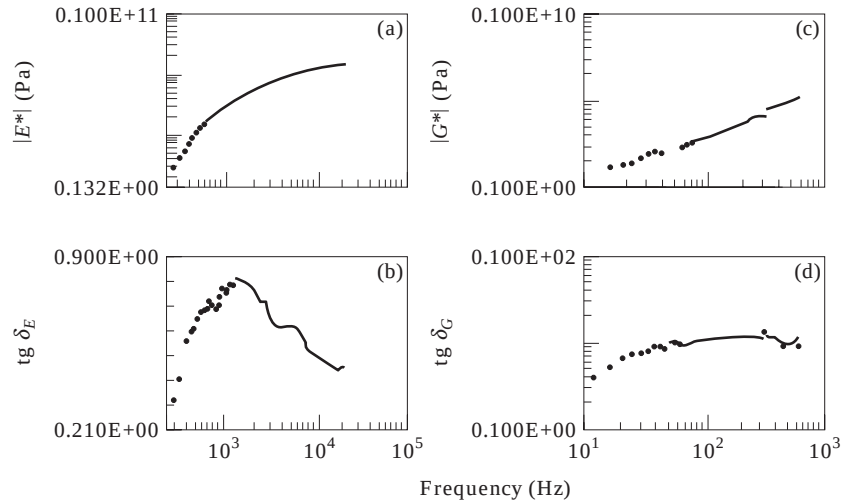

Figure 9. High damping elastomer. (a) Young's modulus (absolute value); (b) damping coefficient tg δ_E; (c) shear modulus (absolute value); (d) damping coefficient tg δ_G.

with many maxima and on the Young's modulus (in absolute value) by the presence of different slopes.

7.2.3. *Correcting Young's modulus by using equation* (38)

For materials with low damping coefficients, the resonance frequencies can be high and the correcting formula is necessary, to take into account transverse inertia and transverse shear. The apparent modulus E_a^* and the corrected modulus E_c^* are shown in Figure 11.

7.3. TESTS ON LOW DAMPING POLYMERS

For this kind of polymer one can have more than six resonance frequencies. If the complex variable Newton–Raphson method, equations (22) and (23), is used without

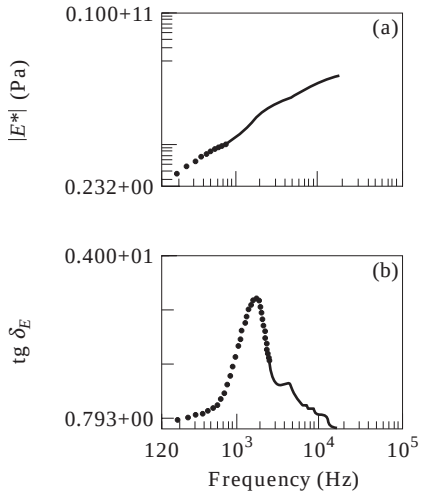

Figure 10. Low damping elastomer. (a) Young's modulus (absolute value); (b) damping coefficient tg δ_E.

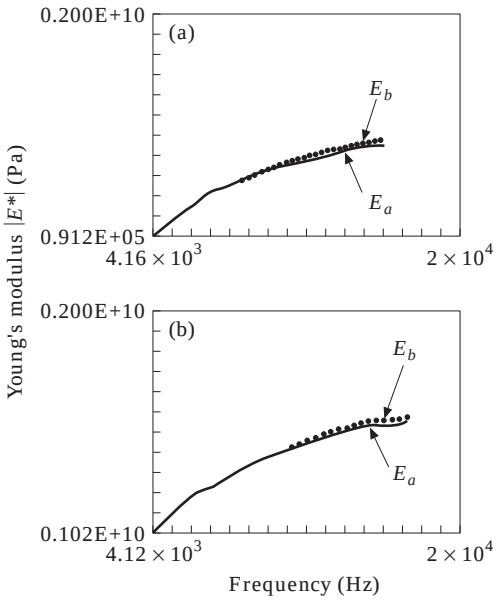

Figure 11. Low damping elastomer. (a) . . . . , Inertia and transverse shear correction; ——, without correction. (b) . . . . , Length correction; ——, without correction.

caution, one can obtain E^* curves with parasitic oscillations as presented in Figure 3, particularly for the imaginary part of E^*.

With the improvements proposed for the complex Newton–Raphson method by evaluating E^* directly at resonance and antiresonance frequencies and by evaluation of E^* in frequency intervals with monotonic variation of $|T^*|$, the parasitic oscillations are reduced.

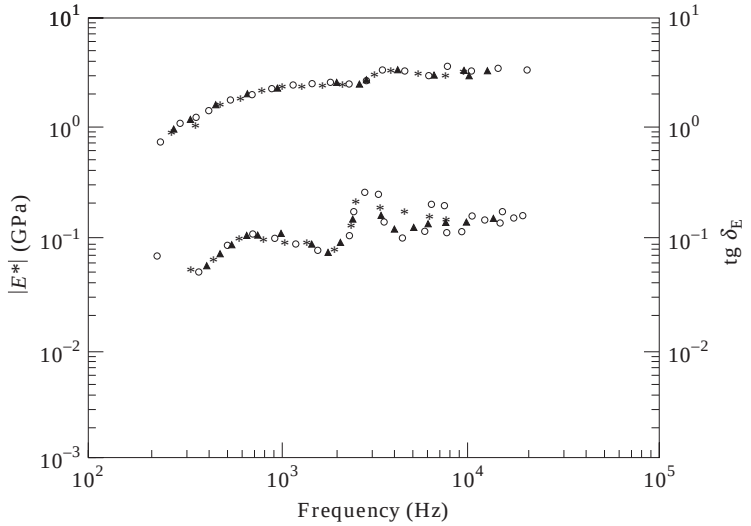

Figure 12. Young's modulus absolute value and damping evaluated by three methods. ○○○○, Newton–Raphson method without division of frequency range into intervals; ▲▲▲▲, Newton–Raphson method with decomposition into frequency intervals excluding resonance and antiresonance frequencies; ********, Black's chart method. Material, polyamide 6 (PA6).

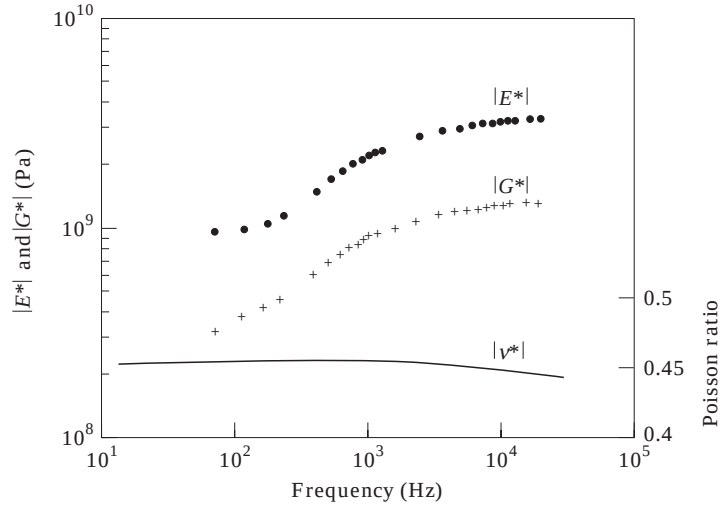

Figure 13. The shear modulus $G^*(f)$ and the Young's modulus $E^*(f)$ are evaluated on the same specimen; Poisson ratio ν^* (from equation (35)). Material, polyamide (PA6). The Poisson ratio is practically constant over the range of frequencies presented.

In Figure 12 is presented the Young's modulus of polyamide 6 (PA6), as obtained from the Newton–Raphson method (equations (22)); the parasitic oscillations are visible on the curve $|E^*|$. Figure 12 is obtained from results presented in Figure 2.

Using Black's chart as presented in Figure 4 one obtains the monotonically increasing Young's modulus shown in Figure 11.

The Young's and shear moduli can be obtained on the same specimen. The variations of $|E^*|$ and $|G^*|$ versus frequency are shown in Figure 13.

Poisson's ratio is practically constant in the range of frequency 100–10 000 Hz.

8. CONCLUDING REMARKS

Complex moduli (Young's and shear) can be obtained over a large range of frequency, exceeding three decades, by measuring transmissibility function with many resonance and antiresonance frequencies.

The same samples are used to evaluate both moduli E^* and G^*.

The experimental set-up is simple to realize. Boundary conditions adopted (free end with additional mass or inertia) also are simple to obtain. It is not necessary to have a rigid frame as in the impedance method.

Two Newton–Raphson methods have been used and discussed with appropriate cautions to avoid oscillations of the complex moduli curves.

Black's chart is a new method to evaluate complex moduli.

Correction formulae are available to obtain correct values of complex moduli at higher frequency.

ACKNOWLEDGMENTS

The authors gratefully acknowledge the two anonymous reviewers who gave us additional references and indicated some errors. Their pertinent remarks were accounted for in the final manuscript.

REFERENCES

1. J. D. Ferry 1970 *Viscoelastic Property of Polymers*. New York: John Wiley; second edition.
2. S. Oyadiji and G. R. Tomlinson 1996 *Journal of Sound and Vibration* **186**(4), 623–647. Characterization of the dynamic properties of viscoelastic elements by the direct stiffness and master curve methodologies, part 1: design of load frame and fixtures.
3. J. S. Snowdon 1968 *Vibration and Shock in Damped Mechanical System*. New York: John Wiley.
4. T. Pritz 1981 *Journal of Sound and Vibration* **77**, 93–100. Apparent complex Young's modulus of a longitudinally vibrating viscoelastic rod.
5. B. R. Read and G. D. Dean 1978 *The Determination of Dynamic Properties of Polymers and Composites*. Bristol: Adam Hilger.
6. S. O. Oyadiji and G. R. Tomlinson 1985 *Journal of Sound and Vibration* **101**, 277–298. Determination of the complex moduli of viscoelastic structural element by resonance and non-resonance methods.
7. B. Lundberg and R. H. Blanc 1988 *Journal of Sound and Vibration* **126**, 97–108. Determination of material properties from the two-point response of an impacted linearly viscoelastic rod specimen.
8. S. Ödeen and B. Lundberg 1993 *Journal of Sound and Vibration* **165**, 1–8. Determination of complex modulus from measured end-point accelerations of an impacted rod specimen.
9. T. Beda 1990 *Ph.D. Thesis*, *CNAM*, *Paris*. Modules complexes des materiaux viscoélastiques par essais dynamiques sur tiges—petites et grandes déformations—modélisation (in French).
10. I. Jimeno-Fernadez and H. Uberall 1992 *Journal of the Acoustical Society of America* **91**(4), 2030–2033. Resonance decomposition of the vibratory response of viscoelastic rods.
11. M. Soula 1996 *Ph.D. Thesis*, *CNAM*, *Paris*. Etude du comportement mécanique des matériaux viscoélastiques par les dérivées fractionnaires (in French).
12. D. K. Rao and J. S. Rao 1974 *Journal of the Acoustical Society of America* **56**(6), 1792–1800. Free and forced vibrations of rods according to Bishop's theory.
13. A. D. S. Barr 1962 *Journal of Mechanical Engineering Science* **4**(4), 127–135. Torsionnal waves in uniform elastic rods of non-circular section.
14. T. Vinh 1991 *The Dynamic Properties of Advanced Composites* (Course at ISMCM Saint-Ouen).

APPENDIX A: EXPRESSION FOR μ IN BARR'S EQUATION OF MOTION [13]

The expression for μ is

$$\mu^2 = \frac{b^2}{1+c^2}\left[\frac{c^2}{3} + \frac{768}{\pi^6}\sum_{n=0}^{\infty}\frac{1}{(2n+1)^6}\left[\frac{3\,\mathrm{th}\left((2n+1)\pi\,\frac{c}{2}\right)}{(2n+1)\pi\,\frac{c}{2}} + \mathrm{th}^2\left((2n+1)\pi\,\frac{c}{2}\right) - 3\right]\right].$$

Here b is the width of the sample, $c = b/h$, h being the thickness, and th is the hyperbolic tangent.

The coefficient μ takes into account the warping of the rectangular cross-section.

APPENDIX B: IS THE POISSON RATIO FREQUENCY DEPENDENT OR NOT?

Strictly speaking, for viscoelastic and isotropic material, two complex independent moduli are necessary for mechanical characterization; for example, the Young's modulus $E^*(f)$ and the shear modulus $G^*(f)$. Both moduli, in principle, are frequency dependent. This method of reasoning brings with it many difficulties in the interpretation of experimental results. Equation (34) shows that one has to deal with two unknown

frequency dependent functions $E^*(f)$ and $G^*(f)$ with only one available equation of motion.

Practically, the hypothesis of a constant Poisson ratio is often adopted so as to permit the evaluation of $E^*(f)$. It requires independent measurements of $E^*(f)$ and $G^*(f)$ and the checking of constant v in the range of frequency used. A variety of experiments have been carried out to validate or invalidate this hypothesis [1].

In the present study, the experimental set-up was arranged so as to use an elementary equation of motion (2), subject to the restriction (1). The Poisson ratio is used only in correction formulae (38) and (47).

For elastomers, the Poisson ratio is often supposed to have the value 0·5. That means that the material is incompressible. In reality, elastomers are more or less compressible and the Poisson ratio is less than 0·5.

To find an asymptotic value of v, ultrasonic methods have been used with success [14].

APPENDIX C: NOMENCLATURE

$E^*(f)$, $G^*(f)$	complex Young's and shear moduli	β^*	$= \beta_1 - j\beta_2$, complex wavenumber in equation (12)
$H^*(f)$	transmissibility function	tg δ	damping coefficient (14)
$u^*(x, t)$	harmonic displacement	γ_2	$= M_2/\rho SL$ quotient of the accelerometer mass to the mass of the rod
L	rod length		
b, h	width and thickness of the rod		
f	frequency	v	Poisson ratio
$T^*(f)$	reciprocal of $H^*(f)$	ω	angular frequency
v	phase velocity of wave		